Numerical Methods for Approximating Invariant Manifolds of Delayed Systems

Tuhin Sahai and Alexander Vladimirsky

February 12, 2009

Abstract

In this paper we develop new methods for computing $k-$dimensional invariant manifolds of delayed systems for $k \geq 2$. Our current implementation is built for $k = 2$ only, but the numerical and algorithmic challenges encountered in this case will be also present for any $k > 1$.

For small delays, we consider methods for approximating delay differential equations (DDEs) with ordinary differential equations (ODEs). Once these approximations are made, any existing method for computing invariant manifolds of ODEs can then be used directly. We derive bounds on errors incurred by the most natural of these approximations. For large delays, we extend to DDEs the method originally introduced by Krauskopf and Osinga [1] for invariant manifolds of ODEs. We test the convergence of the resulting algorithms numerically and further illustrate our approach by computing two-dimensional unstable manifolds of equilibria in the context of phase-conjugate feedback lasers.

1 Introduction

Computation of invariant manifolds in ordinary differential equations (ODEs) is an active research area with a variety of numerical approaches and many practical applications. Invariant manifolds give great insight into the global dynamics of dynamical systems. Stable and unstable manifolds of invariant sets form a geometric skeleton of dynamics in phase space. E.g., for a system with multiple attractors, a basin boundary can be often recovered as a co-dimension one stable manifold of a saddle point. On the other hand, non-transverse intersections of stable and unstable manifolds give rise to homoclinic and heteroclinic bifurcations. Several numerical methods for approximating higher-dimensional[1] invariant manifolds of ODEs have been developed over the years [1, 2, 3, 4, 5]; a recent overview and comparison of these can be found in [6]. For delay differential equations (DDEs), an algorithm for computing one-dimensional invariant manifolds (in the Poincaré map) of periodic orbits has

[1]The key challenge addressed by these methods is the "geometric stiffness" (discussed in section 2), typically arising in all but one-dimensional invariant manifold computations. Thus, for the purposes of this paper, the term "higher-dimensional" should be always interpreted as "higher-than-one-dimensional" manifolds.

been introduced by Krauskopf and Green in [7, 8]. Very little, however, has been done so far to approximate higher-dimensional invariant manifolds of DDEs, though some relevant theoretical convergence results can be found in [9].

Delay differential equations are used to model systems where the rate of change depends not only on the present but also on past states of the system, e.g.,

$$\dot{x}(t) = f(x(t), x(t-\tau)). \tag{1}$$

Here $x(t) \in \mathbb{R}^n$ is the current system state, $\tau > 0$ is the delay, and $f : \mathbb{R}^n \times \mathbb{R}^n \mapsto \mathbb{R}^n$ is a smooth function. For applications and examples of delayed systems see [10, 11, 12, 13]. Eqn. 1 is a simplified case: in general there may be multiple and/or state-dependent delays in the system and the derivative terms themselves might also involve delays (leading to "neutral delay equations"). For simplicity, we will restrict our exposition to the case of a single constant delay (as in Eqn. 1) though the case of multiple delays can be treated similarly. Even in this single-delay case, the analysis is significantly harder than for ODEs since the phase space is now infinite-dimensional (the Banach space $\mathcal{C}$ of continuous functions from the delay interval $[-\tau, 0]$ to $\mathbb{R}^n$); see [14]. We provide a brief overview of DDEs in section 1.1.

In this paper we focus on methods for computing higher-dimensional invariant manifolds of DDEs. Given an initial $(k-1)$-dimensional manifold $\mathcal{M}_0 \subset \mathcal{C}$, it is often necessary to compute the k-dimensional manifold $\mathcal{M}$ by evolving $\mathcal{M}_0$ under the flow defined by Eqn.1. One typical case is when the initial manifold $\mathcal{M}_0$ is chosen in the unstable linearized subspace of an equilibrium. In this case the computed manifold would approximate the unstable manifold of that equilibrium. In contrast, stable invariant manifolds of equilibria in DDEs are infinite-dimensional. However, finite dimensional submanifolds of stable manifolds can also be approximated by similar methods.

We start by discussing a standard method for numerical integration of delayed systems. Given a history $\phi \in \mathcal{C}$, it is easy to integrate the system forward in time [15]. Thus, it is tempting to evolve individual points on $\mathcal{M}_0$ and to approximate $\mathcal{M}$ with a finite number of such trajectories. However, the efficiency of such a method is low due to a non-uniform rate of separation of trajectories inside the manifold. This phenomenon of "geometric stiffness" is described in section 2. We note that a similar challenge already arises even for ODEs, and a number of algorithms have been developed to get around this difficulty [1, 2, 3, 4, 5]. In section 3 we show that a small-delay DDE can be approximated by the corresponding ODE system, thus making these prior methods directly applicable. However, when the delay is large, this simple ODE-approximation becomes inaccurate while its natural generalization (section 4.1) is often prohibitively expensive. In section 4.2, we introduce a new/alternative approach for the large-delay case: we extend to DDEs the method originally introduced by Krauskopf and Osinga for ODEs [1]. We note that our discussion of approximation errors and of computational cost of various algorithms is valid for any $k \geq 2$, but our current implementation of the algorithm in section 4.2 assumes $k = 2$.

We illustrate and compare the above approaches by computing several 2-dimensional unstable manifolds of equilibria. Numerical experiments are used to test the convergence of our methods in section 5.1 for an explicitly known invariant manifold. In section 5.2 we use the Arneodo system [16] with an artificial delay to show that our methods can also be used

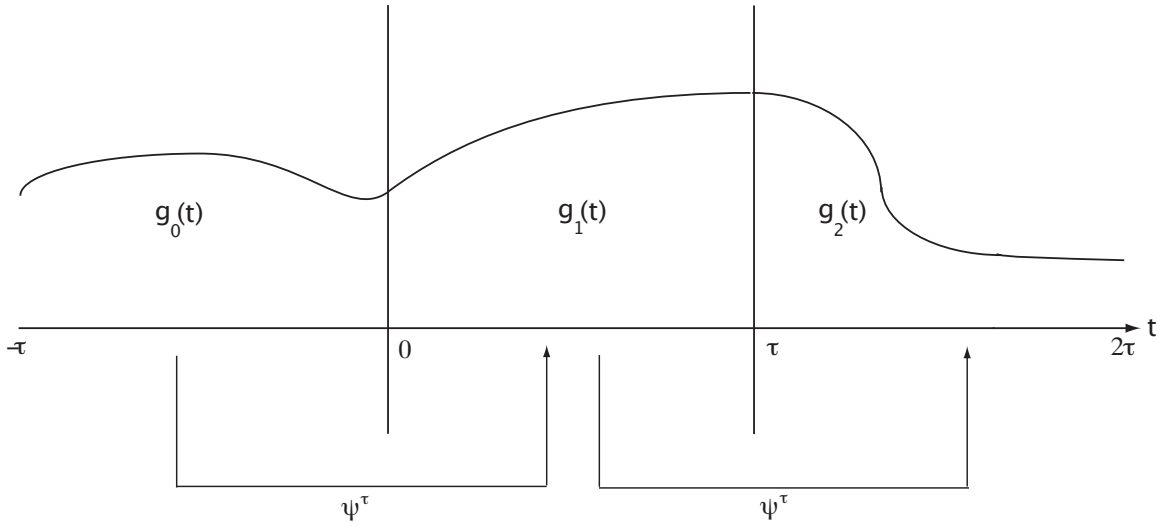

Figure 1: The flow of a DDE (denoted by ψ^τ) maps functions from one τ interval to another.

to compute manifolds accumulating on limit cycles. Our last example (in section 5.3) shows the usefulness of these new methods for analyzing the dynamics of phase-conjugate feedback (PCF) laser systems previously studied by Green, Krauskopf and collaborators [17, 8, 7, 18]. We conclude by discussing the limitations of our approach and list several topics for future research in section 6.

1.1 Delay differential equations: an overview

Eqn. 1 is posed on an n-dimensional physical space, but its phase space $\mathcal{C}$ is infinite-dimensional; to initialize the system, $x(t)$ has to be specified on the interval $[-\tau, 0]$ since $x(0)$ alone is insufficient to define the evolution. For any given history $\phi \in \mathcal{C}$, we can numerically integrate the system given by Eqn. 1 to obtain its future state $x(t, \phi)$ [15]. Let $\psi^t : \mathcal{C} \mapsto \mathcal{C}$ be the flow for Eqn. 1 (see Fig. 1). Our general goal is to start with a $(k-1)$-dimensional manifold, $\mathcal{M}_0$ of points along with their histories and generate a k-dimensional manifold $\mathcal{M} = \psi^t(\mathcal{M}_0)$.

A point $x_0 \in R^n$ is an equilibrium of Eqn. 1 if

$$f(x_0, x_0) = 0. \tag{2}$$

The above equation guarantees that, if the system spends τ seconds at state x_0, it will remain there indefinitely. The stable and unstable invariant manifolds of equilibria are defined as usual [14]:

$$W^s(x_0) = \{\phi \in \mathcal{C} : x(t, \phi) \to x_0 \,\text{as}\, t \to \infty\} \tag{3}$$

$$W^u(x_0) = \{\phi \in \mathcal{C} : x(t, \phi) \to x_0 \,\text{as}\, t \to -\infty\}\,. \tag{4}$$

We note that in general backward time integration is not always possible for DDEs. However, if $\phi \in W^s(x_0)$ or $W^u(x_0)$, the conditions for backward continuation are satisfied [14].

Eqn. 1 can be linearized about the equilibrium x_0 to obtain

$$\dot{x}(t) = Ax(t) + Bx(t-\tau), \tag{5}$$

where A and B are the Jacobian matrices with respect to $x(t)$ and $x(t-\tau)$, respectively; i.e.,

$$A(i,j) = \left[\frac{\partial f_i}{\partial x_j(t)}\right]_{x=x_0}; \qquad B(i,j) = \left[\frac{\partial f_i}{\partial x_j(t-\tau)}\right]_{x=x_0}.$$

We can obtain the characteristic equation for Eqn. 5 by looking for solutions of the form $x(t) = e^{\lambda t}$ [14, 19].

$$\Delta(\lambda) \equiv \det\left(\lambda I - A - Be^{-\lambda\tau}\right) = 0. \tag{6}$$

The roots (eigenvalues) λ of the characteristic equation (Eqn. 6) determine the local stability of the equilibrium. The corresponding eigenvectors $v \in \mathbb{R}^n$ satisfy

$$(\lambda I - A - Be^{-\lambda\tau})v = 0. \tag{7}$$

If $Re(\lambda) > 0$ for any of the eigenvalues, the equilibrium is unstable. Since the characteristic equation (Eqn. 6) is transcendental, it has infinitely many eigenvalues, but the number of eigenvalues in Eqn. 6 with $Re(\lambda) > 0$ is finite [14]. If $Re(\lambda) \neq 0$ for all eigenvalues, then the space $\mathcal{C}$ can be decomposed into $E^u \oplus E^s$, where E^u is the set of initial histories of solutions of Eqn. 5 that approach the equilibrium as $t \to -\infty$. Similarly, E^s is the set of initial histories of solutions of Eqn. 5 that approach the equilibrium as $t \to \infty$ [14]. Moreover, $W^s(x_0)$ and $W^u(x_0)$ are tangential to E^s and E^u respectively (at the equilibrium point x_0) [14].

2 Computation of unstable manifolds via numerical integration of individual trajectories

A variety of methods exist for numerical integration of individual trajectories of DDEs [15]. For example, MATLAB now has a standard implementation of a DDE solver called `dde23` [20]. The extension of standard Runge-Kutta methods to DDEs is quite natural. All numerical integration used in this work is done by using a constant stepsize fourth order Runge-Kutta scheme. We start with $x(t)$ known on the interval $[-\tau, 0]$. This initial history is discretized at intervals of $\frac{h}{2}$, where h is the stepsize of the scheme. We then compute $x(h)$ using the constant stepsize Runge-Kutta scheme [15]. The fourth order Runge-Kutta requires that we evaluate the function $f(x(t), x(t-\tau))$ at the midpoints of the h-sized intervals. So, while computing $x(\tau + \frac{h}{2})$ we will need the value of $x(\frac{h}{2})$. For this reason, after computing $x(h)$ we use a cubic polynomial interpolation (suitable for preserving the uniform 4th-order accuracy of RK4) to compute and store the value of $x(\frac{h}{2})$. This procedure of advancing the solution by h and interpolating to get the value at $\frac{h}{2}$ is then repeated for the entire length of the computed trajectory.

For systems with a one-dimensional unstable manifold (i.e. only one unstable root for Eqn. 7), that unstable manifold can be computed quite easily. We can choose the initial

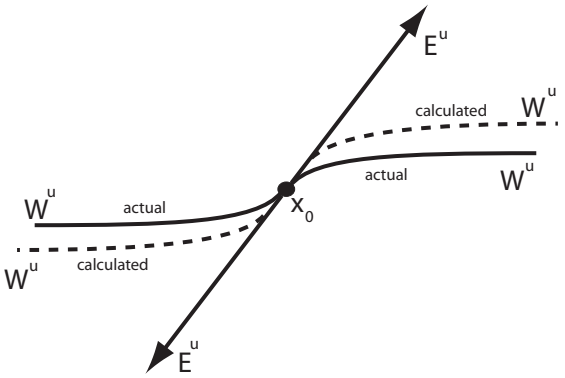

Figure 2: Algorithm for computing 1 dimensional manifolds in delayed systems.

history in the unstable linearized subspace (E^u) and then simply integrate it forward in time to obtain an approximation for the unstable manifold (W^u). This idea is illustrated in Fig. 2.

We now assume that ($Re(\lambda_i) > 0$) only for $i = 1, \ldots, k$; this corresponds to a k-dimensional manifold $W^u(x_0)$. For $k \geq 2$, a naive method for computing $W^u(x_0)$ consists of choosing a large number of histories in E^u and computing the corresponding DDE-trajectories. Such initial histories have the form $c_1 e^{\lambda_1 t} v_1 + c_2 e^{\lambda_2 t} v_2 + \ldots + c_k e^{\lambda_k t} v_k$, where c_i's are arbitrary (sufficiently small) constants, λ_i's are the unstable eigenvalues, and v_i's are the corresponding eigenvectors. After these initial histories are chosen, one can integrate all trajectories numerically up to a specified time T. It has been shown that the discretized version of each such trajectory is close to the actual unstable manifold of delayed systems, provided the discretization step h is sufficiently small [9]. Unfortunately the phenomenon of *geometric stiffness* usually makes the above approach inefficient: the rate of separation of trajectories within the manifold is quite often highly non-uniform resulting in an oversampling of some parts of the manifold and a severe undersampling elsewhere. To illustrate this point, consider a simple system of DDEs with an equilibrium at the origin:

$$\begin{aligned} \dot{x}_1(t) &= x_1(t) + e^{\lambda_1 \tau} x_1(t-\tau)(\lambda_1 - 1)\,, \\ \dot{x}_2(t) &= x_2(t) + e^{\lambda_2 \tau} x_2(t-\tau)(\lambda_2 - 1)\,, \\ \dot{x}_3(t) &= x_3(t) + e^{\lambda_3 \tau} x_3(t-\tau)(\lambda_3 - 1)\,. \end{aligned} \tag{8}$$

It is easy to see that $x_1(t) = C_1 e^{\lambda_1 t}$, $x_2(t) = C_2 e^{\lambda_2 t}$ and $x_3(t) = C_3 e^{\lambda_3 t}$ are solutions for this system of equations. If we pick $\lambda_1 = 2$, $\lambda_2 = 1$ and $\lambda_3 = -1$, the (x_1, x_2) plane becomes an unstable manifold (for all $\tau > 0$). For illustrative purposes, we set $\tau = 1$ and choose a small circle centered at the origin in the (x_1, x_2) plane to generate a finite number of equidistant initial conditions (along with their histories). We integrate each of them forward until a prescribed time to produce Fig. 3(a). We note that on a typical trajectory x_1 grows much faster than x_2; the resulting finite collection of trajectories provides a very poor approximation of the manifold.

An improvement on the above time integration method would be to do arclength integration (similarly to what was done in [3] for the ODEs). The trajectory arclength $s(t)$ satisfies

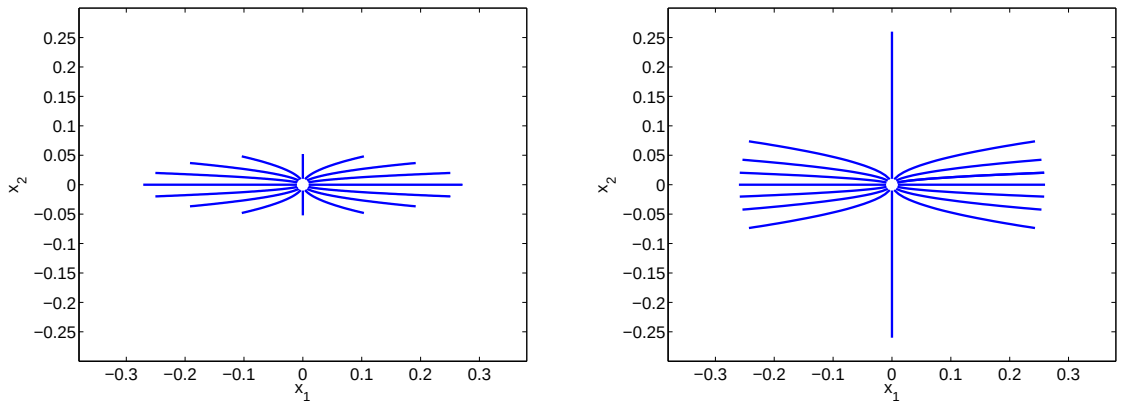

(a) (b)

Figure 3: Fourth order Runge-Kutta integration in (a) time and (b) arclength on Eqn. 8 with $\lambda_1 = 2$, $\lambda_2 = 1$, $\lambda_3 = -1$ and $\tau = 1$.

$\frac{ds}{dt} = \|\frac{dx}{dt}\|$. For DDEs this yields the following transformation of Eqn. 1:

$$\begin{aligned} \frac{dx}{ds} &= f\left(x\left(t(s)\right), x\left(t(s)-\tau\right)\right)\frac{dt}{ds}; \\ \frac{dt}{ds} &= \left\|f\left(x\left(t(s)\right), x\left(t(s)-\tau\right)\right)\right\|^{-1}. \end{aligned} \tag{9}$$

By stepping in arclength, instead of time, it becomes easier to generate all trajectories without integrating to large values of time (see Fig. 3(b)). When implementing the arclength integration for DDEs, it is important to store the value of time along the trajectories. This is needed to evaluate $x(t-\tau)$, while computing $f(x(t), x(t-\tau))$. Cubic polynomial interpolation is again used to evaluate the value of $x(t-\tau)$ if $t-\tau$ falls in between two stored points along the arclength. However, the geometric stiffness is still evident in Fig. 3(b) (after all, the trajectories are simply reparametrized and their rate of separation is the same as before). For ODEs, Johnson et al. [3] get around this problem, by redistributing points along the geodesic distance level sets that represent the manifold. This, however, can be computationally expensive and leads to additional interpolation errors.
We now look at methods for computing unstable manifolds of DDEs more closely.

3 Small τ approximation

Given the volume of prior work on computation of invariant manifolds of ODEs [6], the idea of approximating DDEs with ODEs is very attractive. For small delays (i.e., when $\tau \approx h$), a natural approximation is attained as a result of a single backward Euler step:

$$x(t-\tau) \;\approx\; x(t) - \tau f(x(t), x(t-\tau)). \tag{10}$$

If this equation can be uniquely solved for $x(t-\tau)$, i.e., if for every $x \in \mathbb{R}^n$ there exists a unique $\tilde{x}(x)$ such that $\tilde{x} = x - \tau f(x, \tilde{x})$, then a reasonable approximation of the DDE (1) is

provided by

$$\dot{z}(t) \;=\; \tilde{f}(z(t)) \;=\; f(z(t), \tilde{x}(z(t)). \tag{11}$$

For integrating individual trajectories, this approach is generally well known (e.g., see [21, Chapter 5] or [22]), but we propose using it to approximate *higher-dimensional* manifolds of DDEs. In section 5 we combine this approach with the original method of Osinga and Krauskopf [1] to approximate invariant manifolds of Eqn. 1 by computing invariant manifolds of Eqn. 11. Here we derive an upper bound for the distance between trajectories of a DDE and of the approximating ODE. For the sake of notational simplicity we restrict our analysis to linear DDEs, though a similar upper bound can be derived for a more general case.

For a linear DDE in Eqn. 5, the approximation in Eqn. 10 results in

$$\tilde{x}(x) = (I + \tau B)^{-1}(I - \tau A)\, x. \tag{12}$$

Denoting $C = (I + \tau B)^{-1}(I - \tau A)$, we obtain the corresponding ODE

$$\dot{z}(t) = (A + BC)z(t). \tag{13}$$

We now derive an upper bound on $|e(t)| = |x(t) - z(t)|$ assuming that $e(0) = 0$ and both $x(t)$ and $z(t)$ are twice continuously differentiable. (This assumption is reasonable for $x(t)$ since we are approximating a trajectory on an unstable invariant manifold, and the smoothness of a DDE trajectory increases with every $\tau-$shift forward in time [14].) Using Taylor's theorem for $0 \le l \le 1$,

$$\begin{aligned} x(t + l\tau) &= x(t) + l\tau\dot{x}(t) + \frac{l^2\tau^2}{2}\ddot{x}(\xi_1), \quad \text{where} \quad \xi_1 \in [t, t + l\tau]\,, \\ z(t + l\tau) &= z(t) + l\tau\dot{z}(t) + \frac{l^2\tau^2}{2}\ddot{z}(\xi_2), \quad \text{where} \quad \xi_2 \in [t, t + l\tau]\,. \end{aligned} \tag{14}$$

Denoting $M = \ddot{x}(\xi_1) - \ddot{z}(\xi_2)$ we obtain,

$$e(t + l\tau) = e(t) + l\tau(\dot{x}(t) - \dot{z}(t)) + \frac{l^2\tau^2}{2}M. \tag{15}$$

$$\dot{e}(t) = \dot{x}(t) - \dot{z}(t) = Ax(t) + Bx(t-\tau) - Az(t) - BCz(t) = Ae(t) + B\left(x(t-\tau) - Cz(t)\right). \tag{16}$$

Using Taylor's theorem again, we can write $x(t - \tau) = x(t) - \tau(Ax(t) + Bx(t - \tau)) + \frac{\tau^2}{2}M_2$ (where the norm of the vector M_2 is bounded). Solving this equation for $x(t-\tau)$, we obtain

$$x(t - \tau) = (I + \tau B)^{-1}(I - \tau A)x(t) + (I + \tau B)^{-1}\frac{\tau^2}{2}M_2. \tag{17}$$

This, in turn, yields

$$x(t - \tau) - Cz(t) = (I + \tau B)^{-1}(I - \tau A)e(t) + (I + \tau B)^{-1}\frac{\tau^2}{2}M_2; \tag{18}$$

so Eqn. 16 now becomes,

$$\dot{e}(t) = \dot{x}(t) - \dot{z}(t) = Ae(t) + B(I + \tau B)^{-1}(I - \tau A)e(t) + B(I + \tau B)^{-1}\frac{\tau^2}{2}M_2. \tag{19}$$

Substituting Eqn. 19 into Eqn. 15,

$$e(t+l\tau) = e(t)+l\tau\left[Ae(t) + B(I+\tau B)^{-1}(I-\tau A)e(t) + B(I+\tau B)^{-1}\frac{\tau^2}{2}M_2\right]+\frac{l^2\tau^2}{2}M. \quad (20)$$

Denoting $\sigma_1 = ||A||_2$ and $\sigma_2 = ||B||_2$ and assuming that that $\sigma_2\tau < 1$, the triangle inequality yields,

$$\begin{aligned} ||I-\tau A|| &\leq 1+\sigma_1\tau, & (21)\\ 1-\sigma_2\tau &\leq ||I+\tau B||, & (22)\\ \left|\left|(I+\tau B)^{-1}\right|\right| &\leq \frac{1}{1-\sigma_2\tau} = K_1, & (23)\\ \left|\left|(I+\tau B)^{-1}(I-\tau A)\right|\right| &\leq \frac{1+\sigma_1\tau}{1-\sigma_2\tau} = K_2. & (24)\end{aligned}$$

Using the triangle inequality on Eqn. 20, we obtain

$$|e(t+l\tau)| \leq |e(t)|\left(1+l\tau(\sigma_1+\sigma_2K_2)\right) + \left|\sigma_2K_1l\frac{\tau^3}{2}M_2\right| + \left|\frac{l^2\tau^2}{2}M\right|. \quad (25)$$

Using the notation $\beta_1 = \sigma_1+\sigma_2K_2$, $\beta_2 = \sigma_2K_1\frac{|M_2|}{2}$ and $\beta_3 = \frac{|M|}{2}$, we can rewrite Eqn. 25 as

$$|e(t+l\tau)| \leq |e(t)|\left(1+l\tau\beta_1\right) + \left|l\tau^3\beta_2\right| + \left|\beta_3l^2\tau^2\right|. \quad (26)$$

Without loss of generality we can assume that $t = m\tau$ (i.e., we are assuming that t is a multiple of τ and we are bounding the error on the interval $[t, t+l\tau]$). Recalling that $\beta_1, \beta_2, \beta_3$ are non-negative, Eqn. 26 becomes

$$|e(t+l\tau)| \leq |e(0)|\,\rho^m(1+l\tau\beta_1)+l\tau^3\beta_2+l^2\tau^2\beta_3+(\tau^3\beta_2+\tau^2\beta_3)(\rho^{m-1}+\rho^{m-2}+\ldots+1), \quad (27)$$

where $\rho = 1+\tau\beta_1$. Since $e(0) = 0$, we see that

$$|e(t+l\tau)| \leq l\tau^3\beta_2 + l^2\tau^2\beta_3 + (\tau^3\beta_2+\tau^2\beta_3)\left(\frac{\rho^m-1}{\rho-1}\right). \quad (28)$$

We note that $\rho^m = (1+\tau\beta_1)^m = (1+\frac{t}{m}\beta_1)^m \leq e^{\beta_1 t}$; thus,

$$|e(t+l\tau)| \leq l\tau^3\beta_2 + l^2\tau^2\beta_3 + \frac{\tau^2\beta_2+\tau\beta_3}{\beta_1}(e^{\beta_1 t}-1). \quad (29)$$

The above equation shows that the error incurred by the approximation at $t+l\tau$ is $O(e^{\beta_1 t})$.

Before switching to the case of large delays, we make several remarks about the approach presented here:

- Since the above bound is an exponential function of time, the resulting approximation is provably useful only in approximating a compact/local subset of the manifold of the original DDE; see section 5 for numerical examples.

- Unlike the approach to be described in section 4.1, here the resulting ODE is still posed in $\mathbb{R}^n$, thus making the approximation computationally attractive.

- The small τ approximation can be similarly extended to the case of multiple constant small delays by setting $\tau_i = m_i\tau$ and $x(t-\tau_i) \approx x(t) - m_i\tau f$.

- If a non-linear DDE is given as a series, then $\tilde{f}$ can be often easily approximated. For example, suppose that

  $$f(x(t), x(t-\tau)) = g(x(t)) + B_1\gamma_1(x(t-\tau)) + B_2\gamma_2(x(t-\tau)) + B_3\gamma_3(x(t-\tau)) + \ldots,$$

  where $g(x(t))$ is an arbitrary function, B_i's are arbitrary constant matrices and $\gamma_i(x) = [x_1^i, \ldots, x_n^i]^T$. Then the small delay approximation yields

  $$\tilde{f}(z) \approx \left(I + \tau\sum_{i=1}^{\infty} iB_iZ^{i-1}(z)\right)^{-1}\left(g(z) + \sum_{i=1}^{\infty} B_i\gamma_i(z)\right),$$

  where $Z = \mathrm{diag}(z_1, \ldots, z_n)$. This approximation can be easily obtained by noting that

  $$\begin{aligned} B_i\gamma_i\left(x(t-\tau)\right) &\approx B_i\gamma_i\left(x(t)\right) - \tau\frac{d}{dt}B_i\gamma_i\left(x(t)\right) \\ &\approx B_i\gamma_i\left(x(t)\right) - \tau B_i i\gamma_{i-1}\left(x(t)\right)\frac{d}{dt}x(t) \\ &\approx B_i\gamma_i\left(x(t)\right) - \tau B_i i\gamma_{i-1}\left(x(t)\right)\tilde{f}. \end{aligned}$$

- Of course, an even simpler (but less accurate) ODE approximation in $\mathbb{R}^n$ results from assuming that $x(t-\tau) \approx x(t)$; e.g., see [22]. The error analysis of the latter has been omitted for the sake of brevity.

4 Algorithms for large delays

We consider two different approaches for computation of invariant manifolds of DDEs when $h \ll \tau$. The first approach (section 4.1) involves approximation of the DDE by a higher-dimensional ODE system and computation of invariant manifolds for the latter system.

The second approach (section 4.2) involves extension of an existing method for computing invariant manifolds of ODEs. We find that two prior algorithms for computing invariant manifolds of ODEs naturally extend to DDEs [1, 3]. Both methods involve integration of the system along trajectories, thus giving easy access to the histories of all stored points and enabling us to compute $f(x(t), x(t-\tau))$ at each such point. Of these two methods, we generalize Krauskopf and Osinga's algorithm rather than the method proposed by Johnson et. al. (The latter method, though also applicable, requires a much more frequent redistribution of points on geodesic curves [3], resulting in a higher computational cost and a faster accumulation of interpolation errors.)

4.1 Approximation of DDEs with higher-dimensional ODEs

We first consider a generalization of the approach discussed in section 3. Since the delay is no longer assumed to be small, a more detailed discretization of the history is needed. Assuming that $h = \tau/N$, the history can be approximated by $x_0, \ldots, x_N$, where $x_i \approx x(t - \tau + ih)$. We note that $\dot{x}_N(t)$ is given by the original DDE, while for all $i < N$, the derivative $\dot{x}_i(t)$ can be approximated by divided differences on the history points. For example, when first order forward differences are employed, this results in a system of ODEs

$$\dot{x}_N = f(x_N, x_0) \qquad \text{and} \qquad \dot{x}_i = \frac{x_{i+1} - x_i}{h} \quad \text{for } i < N. \tag{30}$$

Each x_i $(0 \leq i \leq N)$ is an n dimensional vector (dimension of the physical space), thus giving an $n \times (N+1)$ dimensional system. We note that Eqn. 30 is a *cyclic feedback system*, whose theoretical properties have been well-studied [23, 24]. It is interesting to note that the same system can be obtained from the method of lines discretization of a linear transport PDE approximating Eqn. 1; see [25, 26] and [27].

In principle, it is possible to employ any of the methods in [6] to compute invariant manifolds of Eqn. 30, thus approximating the invariant manifolds of the original DDE. However, for large delays the dimensionality of the resulting system will be large, making this approach prohibitively expensive, especially with methods such as [5], where the computational cost depends on the manifold's co-dimension. We conclude that the method of the next subsection is preferable since it deals with the DDE directly, without increasing the dimensionality of the physical space.

4.2 Direct approximation of invariant manifolds of DDEs

The method of Krauskopf and Osinga [1, 28] approximates a two dimensional invariant manifold of an ODE system using a collection of level-curves of the geodesic distance function on that manifold. Each such geodesic level-curve C_r is discretized by a collection of marker-particles $\{P_i\}$. If $\mathcal{M} = W^u(x_0)$ for some saddle equilibrium x_0, the "initial" curve C_0 can be approximated by taking a circle of radius r_0 in the unstable eigenspace of x_0. If Δ_r is the distance between two adjacent represented level-curves C_r and C_{r+1}, then $(r_0 + \sum_{i=0}^{r-1} \Delta_i)$ can be interpreted as the geodesic distance from x_0 to C_r.

The next level curve (C_{r+1}) is generated by advancing C_r normally to itself (within the manifold) by the distance Δ_r (see Fig. 4). In practice this is accomplished by advancing each $P_i \in C_r$ as follows: if Π_i is the plane orthogonal to the manifold at P_i, a one-dimensional search along C_r is employed to find $p_i \in C_r$, whose trajectory intersects Π_i at a point P_i^* such that

$$\Delta_r(1 - \epsilon) \leq |P_i - P_i^*| \leq \Delta_r(1 + \epsilon).$$

Since p_i is usually not a marker-particle itself, this procedure involves interpolation. The obtained P_i^* is used as a successor of P_i on C_{r+1}. The choice of Δ_r is made based on the manifold curvature as measured on the last computed level curve C_r. To maintain a reasonable representation of the manifold, minimum and maximum distances between

adjacent marker-particles on the geodesic front C_{r+1} are defined to be $\delta_{\min}$ and $\delta_{\max}$. If the distance between P_i^* and P_{i+1}^* falls below $\delta_{\min}$, one of them is deleted; if that distance increases beyond $\delta_{\max}$, a new marker-particle $P_{i+\frac{1}{2}}^*$ is generated as a successor of $P_{i+\frac{1}{2}}$, which is approximated by interpolation on C_r. The front is repeatedly advanced until a predefined geodesic distance is reached along the manifold, or until the manifold converges to a limit set [1]. We refer readers to [28] for further implementation details and for the proof of convergence.

We have extended the above algorithm to DDEs by storing each marker-particle P_i along with its history (see Fig. 4). As before, the history is discretized using N equidistant points and the fourth order Runge-Kutta scheme is used to advance an individual point forward in time. The resulting memory requirements of the algorithm are not particularly restrictive since only a few recently computed level-curves are kept in RAM. The initial set of markers and their histories are approximated using the linearization of the DDE near x_0, as explained in section 2. Correspondingly, to approximate a new point on C_r, interpolation is now used both on the marker-particles and their histories. Our current implementation allows approximation of two-dimensional invariant manifolds of DDEs only. In that case, finding p_i still involves a one-dimensional search along C_r only (which we implemented using a simple bisection algorithm). The extension of this method to higher-dimensional manifolds is conceptually straight-forward [28], but finding p_i will then have to be accomplished by continuation or by solving the corresponding boundary value problem. Our implementation uses $\epsilon = 0.01$, $\delta_{\min} = \Delta/2$, and $\delta_{\max} = 2\Delta$. We note that the above algorithm exploits a combination of ideas in [1, 28] with those in the work of Green and Krauskopf on approximating one-dimensional unstable manifolds of periodic orbits of DDEs [7].

5 Numerical Examples

5.1 Convergence of Numerical Methods

To test the convergence of our algorithms numerically, we use an example where the manifold is a priori known. Consider a system of the form

$$\begin{aligned}
\dot{x}(t) &= \eta_1 x(t-\tau), \\
\dot{y}(t) &= \eta_2 y(t-\tau), \\
\dot{z}(t) &= -\mu z(t-\tau) + \mu g(x(t-\tau), y(t-\tau)) + \eta_1 x(t-\tau) g_x(x(t), y(t)) \\
&\quad + \eta_2 y(t-\tau) g_y(x(t), y(t)),
\end{aligned} \tag{31}$$

where $g(x, y)$ is a smooth function. If $g_x(0, 0) = 0$ and $g_y(0, 0) = 0$, the equilibrium $O = (0, 0, g(0, 0))$ is a saddle for $\eta_1 > 0$, $\eta_2 > 0$ and $\mu > 0$. This is easily checked by linearizing the equation about O, yielding

$$\dot{v}(t) = Bv(t-\tau),$$

where $v(t) = [x(t), y(t), z(t)]^T$, and $B = \mathrm{diag}(\eta_1, \eta_2, -\mu)$. The characteristic equation thus becomes

$$\Delta(\lambda) \equiv \det\left(\lambda I - Be^{-\lambda\tau}\right) = 0. \tag{32}$$

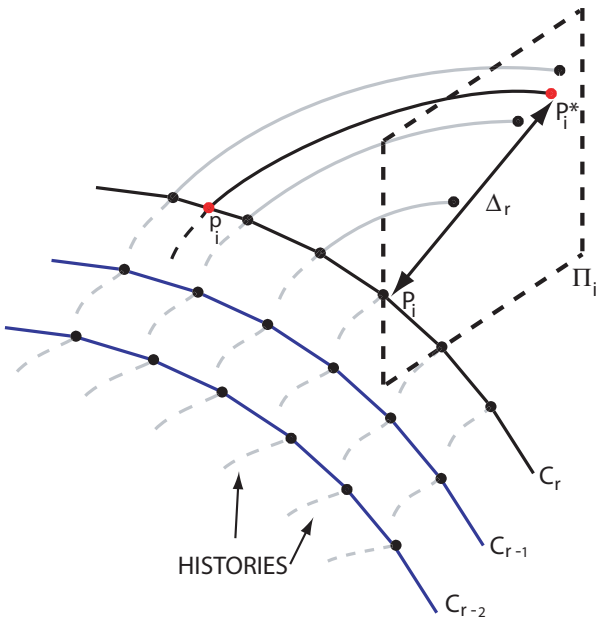

Figure 4: Algorithm for computing geodesic curves. C_r is the present curve, P_i is the point to be advanced, Δ is the distance the geodesic curves are to be advanced and Π_i is the plane orthogonal to C_r at P_i. Dotted lines represent the histories of the points on C_r.

Table I: Convergence for $\mu = 1.0$

R_{init}	$\mu = 1$	
	L_2 error	L_∞ error
$r_0 = 0.2$	4.3675×10^{-6}	8.00856×10^{-5}
$r_0 \times 2^{-1}$	2.3681×10^{-6}	4.16508×10^{-5}
$r_0 \times 2^{-2}$	1.0563×10^{-6}	2.57103×10^{-5}
$r_0 \times 2^{-3}$	5.021×10^{-7}	1.3591×10^{-5}

Table II: Convergence for $\mu = 0.25$

R_{init}	$\mu = 0.25$	
	L_2 error	L_∞ error
$r_0 = 0.2$	5.1430×10^{-5}	6.71421×10^{-4}
$r_0 \times 2^{-1}$	2.9173×10^{-5}	3.83010×10^{-4}
$r_0 \times 2^{-2}$	1.4132×10^{-5}	1.93001×10^{-4}
$r_0 \times 2^{-3}$	7.822×10^{-6}	9.2381×10^{-5}

We note that O is a saddle equilibrium with a two-dimensional unstable manifold $W^u(O)$ coinciding with the graph of $g(x, y)$ in the physical space.

We now use the method of section 4 to approximate $W^u(O)$ for $g(x, y) = x^2 + y^2$ and for particular choices of parameter values. The choice of $\eta_1 = \eta_2 = \mu = \tau = 1$ yields a repeated unstable eigenvalue of Eqn. 32 at $\lambda \approx 0.567142$. The corresponding eigenvectors are $v_1 = [1, 0, 0]^T$, and $v_2 = [0, 1, 0]^T$. We approximate the manifold up to the geodesic distance 1 from the origin, and then calculate the difference between the computed z and $g(x, y)$ on the last geodesic circle. In this experiment we test the convergence by decreasing the radius of the initial circle r_0, while all other accuracy parameters are fixed as described in section 4. Table I shows that both the L_2 and L_∞ errors decrease as $O(r_0)$. The errors (though not the rates of convergence) are also clearly influenced by the value of μ, as illustrated by Table II. The computed manifold is shown in Fig. 5.

We can also use this opportunity to compute the error incurred by the small delay

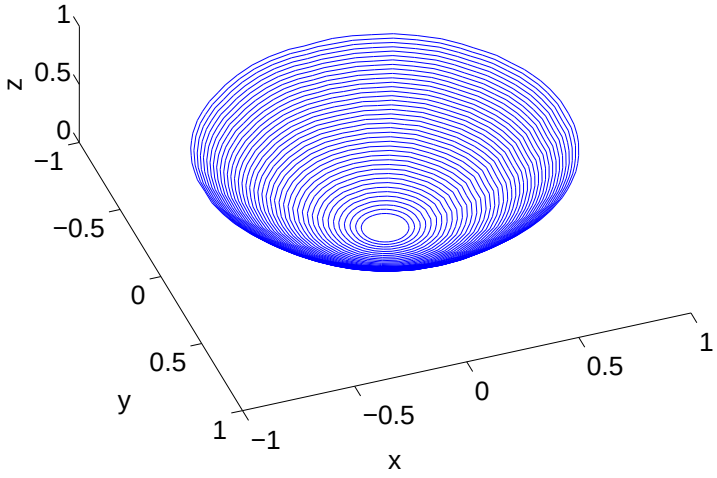

Figure 5: Invariant manifold for the case $g(x, y) = x^2 + y^2$ in Eqn. 31 with $\tau = 1.0$.

approximation of the system described by Eqn. 31. A small τ approximation yields

$$\begin{aligned}
\dot{x} &= \frac{\eta_1 x}{1+\eta_1\tau} \\
\dot{y} &= \frac{\eta_2 y}{1+\eta_2\tau} \\
\dot{z} &= \frac{1}{1-\mu\tau}\left[-\mu z + \mu\left((\frac{x}{1+\eta_1\tau})^2 + (\frac{y}{1+\eta_2\tau})^2\right) + 2\eta_1\frac{x^2}{1+\eta_1\tau} + 2\eta_2\frac{y^2}{1+\eta_2\tau}\right]. \quad (33)
\end{aligned}$$

Using our implementation of Krauskopf and Osinga's original method [28] with the same

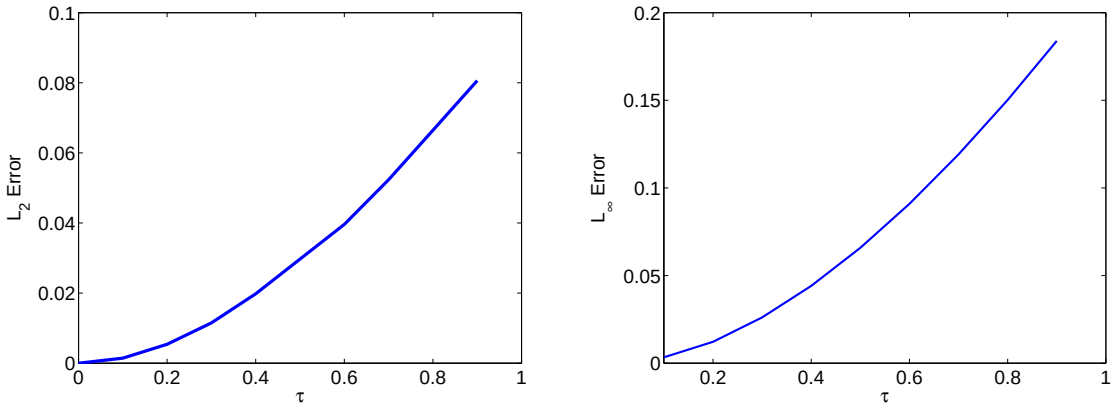

(a) (b)

Figure 6: L_2 and L_∞ errors for the small τ approximation with varying delay.

accuracy parameters, we compute the manifold for Eqn. 33 and measure the errors due to

this approximation for different values of τ. The manifold is approximated up to the geodesic distance of 1.5, and the L_2 / L_∞ errors are measured for the last geodesic level curve. As expected, increasing τ increases the errors induced by the ODE approximation; see Fig. 6.

For the large-delay method of section 4, τ does not influence the accuracy directly provided the history is well-resolved. The latter requirement could be strenuous for large delays. Therefore, it is of interest to explore the dependence of errors on τ if we are restricted to a fixed number of points in the history (i.e., holding $\tau/h = 1500$ and varying h). The results of this experiment for system (31) are shown in Fig. 7. We note that in all the other experiments of this section, the Runge-Kutta step size is held constant at $h = 10^{-3}$ by varying the total number of points in the history.

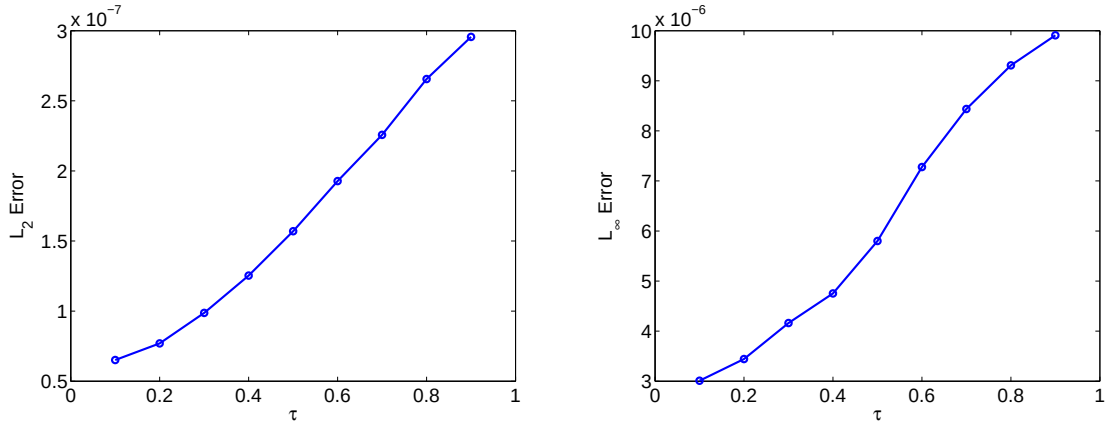

(a) (b)

Figure 7: L_2 and L_∞ errors for the large delay method of section 4 computed for various τ using a fixed number of points in the history.

5.2 Arneodo system with delay

When the geodesic distance on the invariant manifold is bounded from above (e.g., due to the manifold's accumulation on a limit cycle), the algorithm of section 4.2 has to be adjusted, since that limit cycle itself is usually not a geodesic level curve. For ODEs this situation is exemplified by the Arneodo system [16], and we introduce an artificial delay to obtain

$$x''' + x'' + 2x'(t-\tau) - \alpha x + x^2 = 0. \tag{34}$$

The above equation can be recast into,

$$\begin{aligned} \dot{x} &= y \\ \dot{y} &= z \\ \dot{z} &= -z - 2y(t-\tau) + \alpha x - x^2. \end{aligned} \tag{35}$$

For $\tau = 0$ the system has been studied extensively (e.g., [1],[3]). For the undelayed case, the equilibrium points are $O = (0, 0, 0)$ and $A = (\alpha, 0, 0)$. The second equilibrium is attracting

for $\alpha < 2$. At $\alpha = 2$ the equilibrium A loses stability to become a saddle, and the system undergoes a Hopf bifurcation. The two dimensional unstable manifold of A converges to the limit cycle born at $\alpha = 2$ [1, 3] (see Fig. 9). We are interested in how the unstable manifold of point A changes as τ is varied.

Using DDE-BIFTOOL [29], we find that on increasing the delay τ from 0 in Eqn. 35, the Hopf bifurcation occurs at lower and lower values of α. Fixing $\alpha = 2.5$, we see that the increase in τ, results in an increase in the limit cycle amplitude, (Fig. 8(a)), and at $\tau \approx 0.11$ the cycle loses stability at a period-doubling bifurcation. The period-doubled orbit can be clearly seen by numerically integrating the system, Eqn. 35 for $\tau > 0.11$ (Fig. 8(b)).

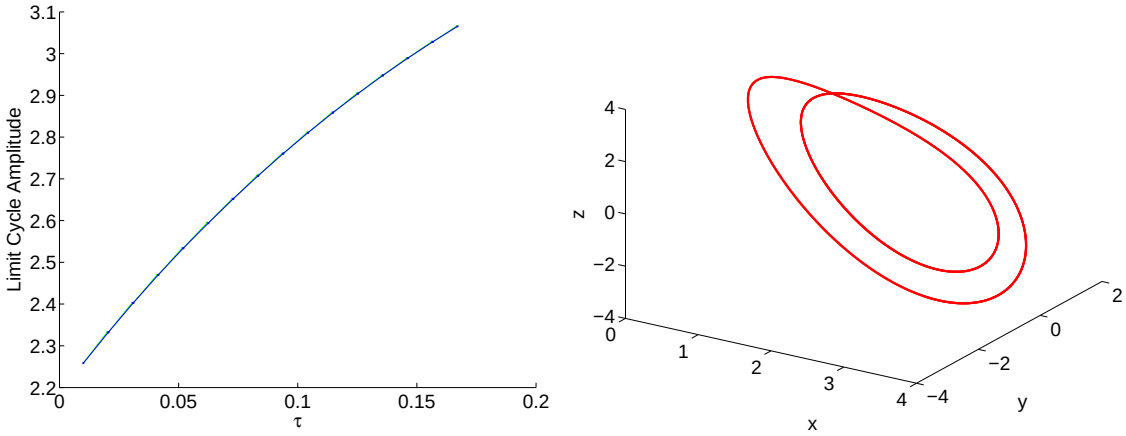

(a) Limit cycle amplitude versus τ at $\alpha = 2.5$. (b) Period-doubled limit cycle at $\tau = 0.13$.

Figure 8:

We now use the algorithm described in the previous section to compute $W^u(A)$ at different values of τ. Since the manifold is bounded by a limit cycle, a convergence process has to take place when the geodesic distance level curves approach the limit cycle [1]. To ensure this we modify the above algorithm to search for the maximum distance $\Delta(P_i) \leq \Delta$ that the point P_i can be advanced by. If the manifold cannot be advanced by a certain predefined distance, the point is accepted as the boundary of the manifold. The stepsize used in the fourth order Runge-Kutta scheme that forms the core of the algorithm is $h = \frac{\tau}{N}$. where N is the number of points stored in the history for each point on the geodesic curve. For the purpose of these simulations $h = 10^{-4}$ and N is changed based on the delay τ. The distance with which the geodesic front is advanced by is initially set to $\Delta = 0.02$, which is then adapted based on the curvature of the manifold. In these experiments we set the accuracy parameters to $\epsilon = 0.01$, $\delta_{\max} = 0.1$, and $\delta_{\min} = 0.01$.

For $\tau = 0$ we find that the manifold converges to the limit cycle as expected [3, 1] as seen in Fig. 9. For $\tau = 0.01$ we find that the manifold again converges to the periodic orbit (see Fig. 10), and the size of the orbit (and hence the manifold) is slightly larger than the case for $\tau = 0$, which is consistent with Fig. 8(a). As we increase τ, we find that the curvature of the manifold increases steadily (e.g., see Fig. 11). On increasing the delay past the period-doubling bifurcation, we find that the manifold has such high curvature that the adjusted Δ falls below the tolerance values and we are unable to compute the manifold.

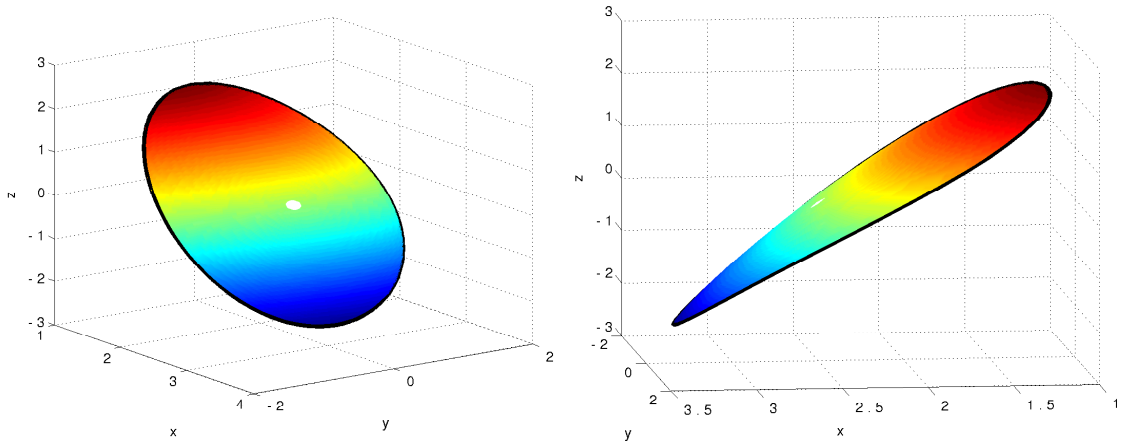

(a) (b)

Figure 9: Unstable manifold of $P = (2.5, 0, 0)$ for the $\tau = 0$ case. The unstable manifold is bounded by the limit cycle (curve in black). Colors depict the z coordinate of the manifold.

We can also compare this result with the small τ approximation (particularly suitable since the manifold is compact). As in section 3, the delayed Arneodo system (Eqn. 35) can be approximated by,

$$\begin{aligned} \dot{x} &= y \\ \dot{y} &= z \\ \dot{z} &= -(1-2\tau)z - 2y + \alpha x - x^2. \end{aligned} \tag{36}$$

Here, $y(t-\tau) \approx y(t) - \tau\dot{y}(t)$ or $y(t-\tau) \approx y(t) - \tau z(t)$. We now compute the invariant manifolds for the system of equations given by Eqn. 36. Since the latter is a system of ODEs, the original method of Krauskopf and Osinga [1] is applicable. We find that for $\tau = 0.01$ this results in a manifold very close to what was already obtained by the general method in Fig. 10.

5.3 Laser with Phase-Conjugate Feedback (PCF)

In this section we study the manifolds that arise in systems modeling semiconductor lasers with phase-conjugate feedback (PCF) [17]. In PCF lasers, a current I raises the atoms to an excited state (population denoted by N in the equations below). A part of the subsequently produced laser (fraction determined by κ) is fed back into the system (so as to excite the atoms) using a phase conjugating mirror (PCM). The time taken by the laser to loop from the system to the mirror and back causes a delay τ (see Fig. 12). The resulting model equations are [17],

$$\begin{aligned} \frac{dE}{dt} &= \frac{1}{2}\left[-i\alpha G_N(N(t) - N_{\text{sol}}) + (G(t) - \frac{1}{\tau_p})\right] E(t) + \kappa E^*(t-\tau)\exp[2i\delta(t-\tau/2) + i\phi_{\text{PCM}}] \\ \frac{dN}{dt} &= \frac{I}{q} - \frac{N(t)}{\tau_e} - G(t)\left|E(t)\right|^2, \end{aligned} \tag{37}$$

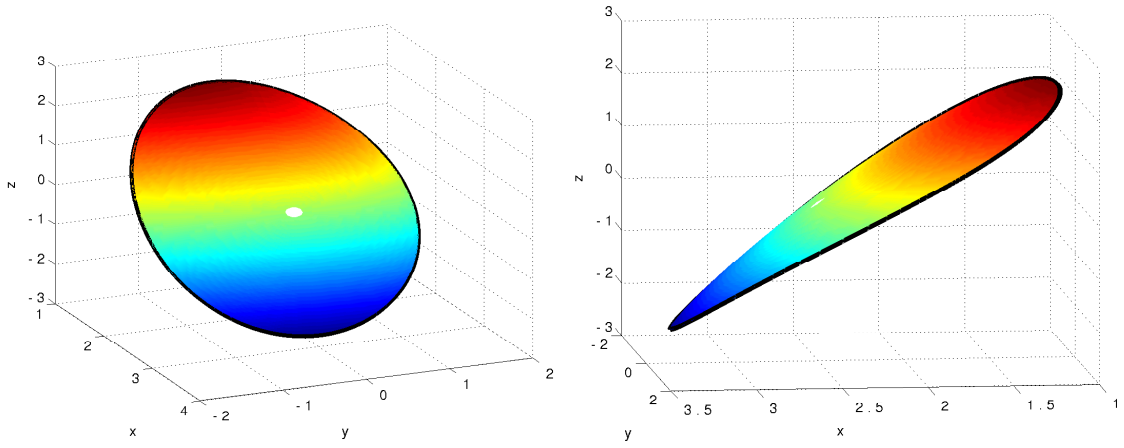

(a) (b)

Figure 10: Unstable manifold of $P = (2.5, 0, 0)$ for the $\tau = 0.01$ case. The unstable manifold is bounded by the limit cycle (curve in black). Colors depict the z co-ordinate of the manifold.

where $E = E_x + iE_y$ is the slowly varying electric field of the laser and E^* is its complex conjugate. The non-linear gain is modeled as

$$G(t) = G_N \left(N(t) - N_0\right) \left(1 - \epsilon \left|E(t)\right|^2\right),$$

with the non-linear gain coefficient $\epsilon = 3.57 \times 10^{-8}$. We use the same parameter values as in [18], corresponding to a Ga-Al-As semiconductor laser: the line-width enhancement factor $\alpha = 3$, the optical gain $G_N = 1190\, s^{-1}$, the photon lifetime $\tau_p = 1.4ps$, the magnitude of the electron charge $q = 1.6 \times 10^{-19}C$, the electron lifetime $\tau_e = 2ns$, and the transparency electron number $N_0 = 1.64 \times 10^8$. The steady-state electron population in the absence of feedback is $N_{\text{sol}} = N_0 + 1/\left(G_N \tau_p\right)$. Following [18] we also assume that both the laser frequency mismatch δ and the constant phase shift ϕ_{PCM} are equal to zero.

This system exhibits "stable periodic operation interspersed with "bubbles" of chaotic dynamics"; it has been previously studied numerically by Krauskopf, Green and co-authors in [17, 8, 7, 18]. The system is posed in (E_x, E_y, N) and possesses $\mathbb{Z}_2$ symmetry corresponding to rotation by π in the complex E plane. As a result, every invariant set is either symmetric or has a symmetric counterpart. A symmetric (trivial) equilibrium x_0 is always present at $(0, 0, I\tau_e/q)$, but becomes unstable at the lasing threshold. Additional non-symmetric saddle equilibria x_1 and x_2 are born as a result of a saddle-node bifurcation. In [18], a two-parameter study of this system using parameters $(\kappa\tau, I)$ shows the evolution of the heteroclinic connection from x_1 to x_2, which gets closer and closer to x_0 and is eventually destroyed at a T-point bifurcation, yielding a codimension-two connection from x_1 to x_0 and a codimension-zero connection from x_0 to x_2. In Figure 13 we show our approximation of $W^u(x_0)$ computed for several points on the branch Het_1 (see [18, Figure 6.1]). In each case we also reproduce the approximation of the heteroclinic connection from x_1 to x_2 computed in [18, Section 7] using the continuation method introduced in [30] and incorporated into

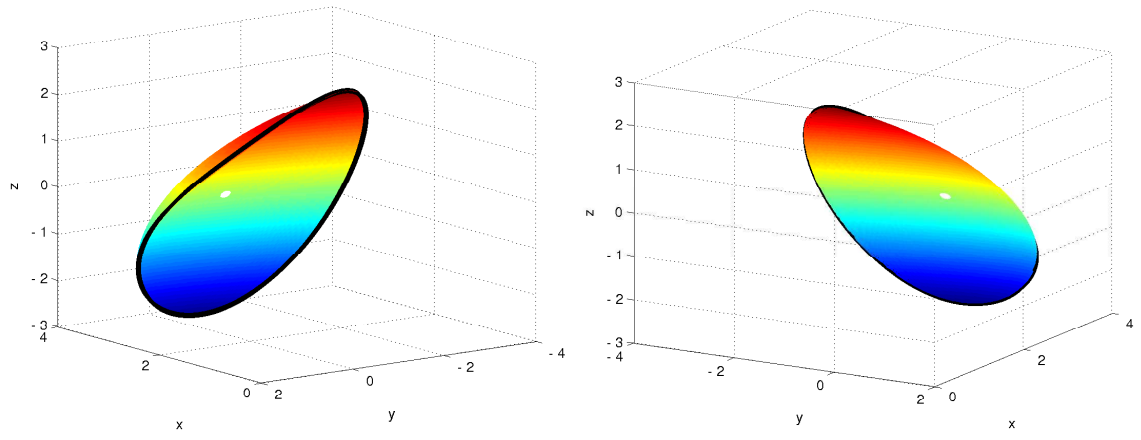

(a) (b)

Figure 11: Unstable manifold of $P = (2.5, 0, 0)$ for the $\tau = 0.08$ case. The unstable manifold is bounded by the limit cycle (curve in black). Colors depict the z coordinate of the manifold. The curvature of the manifold is greater than in the $\tau = 0$ and $\tau = 0.01$ cases.

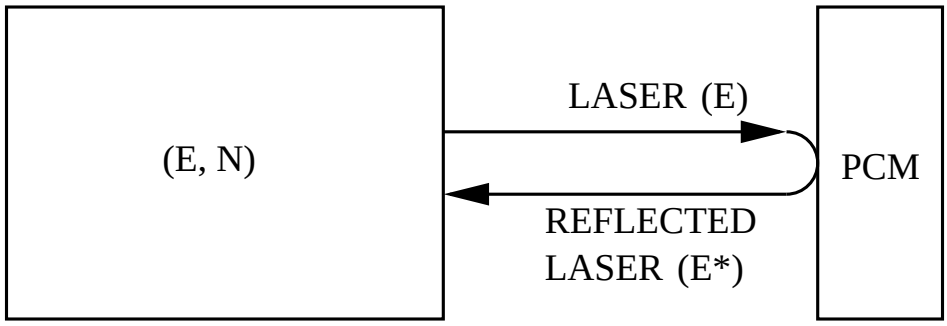

Figure 12: Schematic of the phase conjugating laser feedback.

the software package DDE-BIFTOOL[2]. We note that in this example the delay is "large" – the accuracy needed to resolve a single trajectory leads to using $N = 2500$ points in the history discretizations. Thus, the techniques described in section 3 are inapplicable and we have relied on the method of section 4.2.

6 Conclusions

In comparison to the volume of work that exists for computation of invariant manifolds of ODEs, very little has been done so far to develop efficient methods for approximating

[2]Since for DDEs the phase space is infinite-dimensional, a special integral condition is employed to force the final function segment of the approximate connecting orbit to lie in the complement of the unstable eigenspace of x_2. As noted in [18], "while this integral condition works well in practice, one slight drawback is that it does not control the distance of the end function segment to the steady state." This explains the gap between "the end" of the connecting orbit and x_2 visible in panels of Figure 13.

higher-dimensional invariant manifolds of delay-differential systems. In this paper we develop a methodology for computing invariant surfaces of DDEs. We start with a small delay approximation that approximates the delayed systems with standard ordinary differential equations thus making prior methods for ODEs applicable. We then compute bounds on the global error incurred due to this approximation for an individual trajectory. For the large delay case, we propose a different method, which extends the previous techniques for invariant manifold approximation [28] and does not rely on any direct approximation of the DDE with a system of ODEs. The proposed methods are illustrated using three different numerical examples, including a model for semiconductor lasers with phase-conjugate feedback.

Our current implementation is suitable for two-dimensional manifolds only. In addition, the method is applicable only as long as the geodesic distance function on the manifolds remains smooth. The latter limitation is typical for all methods based on the geodesic distance formulation even in the case of ODEs [28].

In the future we hope to apply our methods to study DDEs arising in control, population biology, and feedback in lasers.

Acknowledgments: The authors would like to thank Koen Engelborghs and Kirk Green for helping with DDE-BIFTOOL. The authors are also indebted to Kirk Green and Bernd Krauskopf for motivating discussions of PCF-laser models and for providing the raw data for the heteroclinic connections shown in Figure 13. This research was supported in part by National Science Foundation grant DMS-0514487.

References

[1] B. Krauskopf and H. M. Osinga. Two-dimensional global manifolds of vector fields. *Chaos*, 9(3):768–774, 1999.

[2] M. E. Henderson. Computing invariant manifolds by integrating fat trajectories. *SIAM Journal on Applied Dynamical Systems*, 4(4):832–882, 2005.

[3] M. E. Johnson, M. S. Jolly, and I. G. Kevrekidis. Two-dimensional invariant manifolds and global bifurcations: some approximation and visualization studies. *Numerical Algorithms*, 14:125–140, 1997.

[4] J. Guckenheimer and P. Worfolk. Dynamical Systems: Some computational problems. In D. Schlomiuk, editor, *Bifurcations and Periodic Orbits of Vector Fields*, pages 241–277. Kluwer Academic Publishers, 1993.

[5] J. Guckenheimer and A. Vladimirsky. A fast method for approximating invariant manifolds. *SIAM Journal on Applied Dynamical Systems*, 3(3):232–260, 2004.

[6] B. Krauskopf, H. M. Osinga, E. J. Doedel, M.E. Henderson, J. Guckenheimer, A. Vladimirsky, M. Dellnitz, and O. Junge. A survey of methods of computing (un)stable manifolds of vector fields. *International Journal of Bifurcation and Chaos*, 15(3):763–792, 2005.

[7] B. Krauskopf and K. Green. Computing unstable manifolds of periodic orbits in delay differential equations. *Journal of Computational Physics*, 186:230–249, 2003.

[8] K. Green, B. Krauskopf, and K. Engelborghs. One-dimensional unstable eigenfunction and manifold computations in delay differential equations. *Journal of Computational Physics*, 197:86–98, 2004.

[9] G. Farkas. Unstable manifolds for RFDEs under discretization: The Euler Method. *Computers and Mathematics with Applications*, 42:1069–1081, 2001.

[10] M. Landry, S. A. Campbell, K. Morris, and C. O. Aguilar. Dynamics of an inverted pendulum with delayed control feedback. *SIAM Journal of Applied Dynamical Systems*, 4(2):333–351, 2006.

[11] D. Pieroux, T. Erneux, T. Luzyanina, and K. Engelborghs. Interacting pairs of periodic solutions lead to tori in lasers subject to delayed feedback. *Phys. Rev. E*, 63:036211, 2001.

[12] C. M. Marcus and R. M. Westervelt. Stability of analog networks with delay. *Phys.l Rev. A*, 39:347, 1989.

[13] J.D. Murray. *Mathematical Biology,Biomathematics texts*, volume 19. Springer-Verlag, 1980.

[14] J. K. Hale and S. M. V. Lunel. *Introduction to Functional Differential Equations.* Springer-Verlag, 1993.

[15] A. Bellen and M. Zennaro. *Numerical methods for delay differential equations.* Oxford Science Publications, first edition, 2003.

[16] A. Arneodo, P. Coullet, E. Spiegel, and C. Tresser. Asymptotic chaos. *Physica D*, 14(3):327–347, 1985.

[17] K. Green and B. Krauskopf. Bifurcation analysis of a semiconductor laser subject to non-instantaneous phase-conjugate feedback. *Optics Communications*, 231:383–393, 2004.

[18] K. Green, B. Krauskopf, and G. Samaey. A two-parameter study of the locking region of a semiconductor laser subject to phase-conjugate feedback. *SIAM Journal on Applied Dynamical Systems*, 2(2):254–276, 2003.

[19] G. Stépán. *Retarded dynamical systems: stability and characteristic functions.* Longman Scientific and Technical, 1989.

[20] L.F. Shampine and S. Thompson. Solving ddes in matlab. *Appl. Numer. Math.*, 37:441–458, 2001.

[21] T.L. Saaty. *Modern Nonlinear Equations.* Dover, New York, 1981.

[22] L.É. Él'sgol'c. *Qualitative methods in mathematical analysis*. Providence, American Mathematical Society, 1964.

[23] T. Gedeon and G. Hines. Upper semicontinuity of morse sets of a discretization of a delay-differential equation. *J. Differ. Equat.*, 151(1):36, 1999.

[24] T. Gedeon and G. Hines. Upper semicontinuity of morse sets of a discretization of a delay-differential equation: an improvement. *J. Differ. Equat.*, 179(2):369, 2002.

[25] A. Bellen and S. Maset. Numerical solution of constant coefficient linear delay differential equations as abstract cauchy problems. *Numerische Mathematik*, 84(3):351–526, 2000.

[26] S. Maset. Numerical solution of retarded functional differential equations as abstract cauchy problems. *J. of Computational and Applied Mathematics*, 161(2):259–282, 2003.

[27] V. Wulf and N.J. Ford. Insight into the qualitative behaviour of numerical solutions to some delay differential equations. In *Proceedings of the fourth Hellenic European Conference on Computer Mathematics and its applications*, volume 2, pages 629–636, 1999.

[28] B. Krauskopf and H. M. Osinga. Computing geodesic level sets on global (un)stable manifolds of vector fields. *SIAM Journal on Applied Dynamical Systems*, 2(4):546–569, 2003.

[29] K. Engelborghs, T. Luzyanina, and G. Samaey. DDE-BIFTOOL v2.00: a Matlab package for bifurcation analysis of delay differential equations. Technical Report TW-330, Department of Computer Science, K.U.Leuven, Leuven, Belgium, 2001.

[30] G. Samaey, K. Engelborghs, and D. Roose. Numerical computation of connecting orbits in delay differential equations. *Numer. Algorithms*, 30:335–352, 2002.

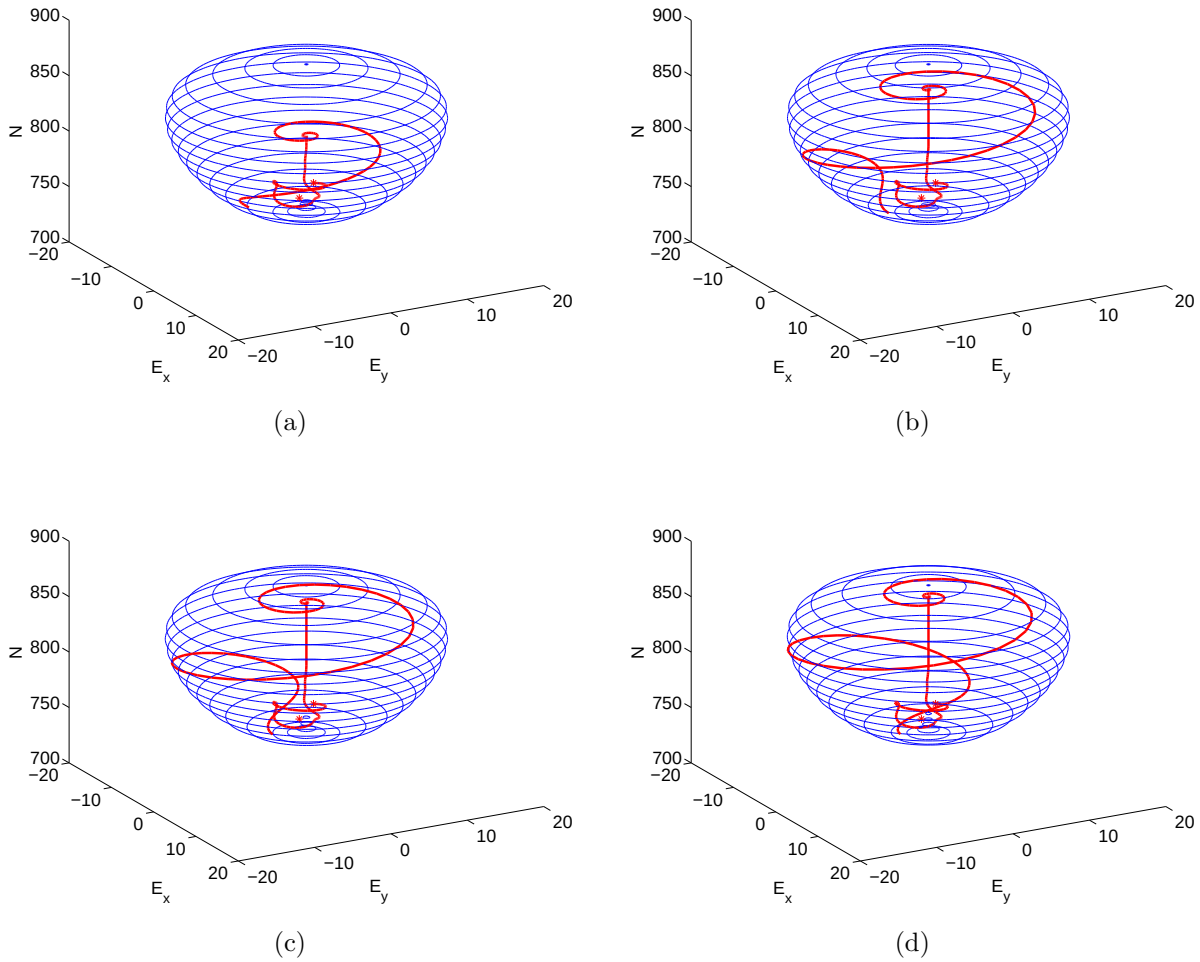

Figure 13: PCF-Laser Example. The unstable manifold of the trivial equilibrium x_0 is shown in blue. Two nonsymmetric saddle equilibria x_1 and x_2 are marked as "*" and their heteroclinic connections are shown in red. In the last panel, the heteroclinic connection passes very close to x_0 and the second half of it nearly lies on the 2D unstable manifold. This is due to the approaching T-point bifurcation, where the connection will split into a codimension-two connection from x_1 to x_0 and codimension-zero connection from x_0 to x_2; see [18] for further details. From (a) to (d), parameters $(\kappa\tau, I)$ take values $(2.1767065, 0.0703938595)$, $(2.1766904, 0.070393885)$, $(2.1767001, 0.070393874)$, and $(2.1766959, 0.070393889)$ respectively.